Winding Design for Minimum Power Loss and Low-Cost Manufacture in Application to Fixed-Speed PM Generator

Rafal Wrobel[1)], Dave Staton[2)], Richard Lock[3)], Julian Booker[3)] and David Drury[1)]

[1)] Department of Electrical & Electronic Engineering
University of Bristol
Bristol, UK
r.wrobel@bristol.ac.uk
d.drury@bristol.ac.uk

[2)] Motor Design Ltd.
Ellesmere, UK
dave.staton@motor-desig.com

[3)] Department of Mechanical Engineering
University of Bristol
Bristol, UK
r.lock@bristol.ac.uk
j.d.booker@bristol.ac.uk

Abstract— **This paper presents results from a coupled thermal and power loss analysis of an open-slot permanent magnet (PM) generator. The research focus has been placed on the winding design providing minimum power loss at ac operation together with low-cost manufacture. The analysed PM generator is intended to operate at fixed-speed allowing for the winding design to be finely tuned for the single operating point. Such a design approach has not been widely reported in the literature, and the existing body of work is focused largely on the variable-speed applications, where the winding design is a compromise between the low- and high-speed operating points, for a given torque speed envelope.**

The ac winding power loss has been analysed for several winding variants with different conductor dimensions accounting for the winding operating temperature. The calculated results suggest that in the analysed PM generator, lower winding slot fill factor is preferable as compared with the more common approach, where the highest manufacturable winding slot fill factor is usually considered. The power loss predictions have been supplemented with thermal analysis of the complete generator assembly for the winding variants considered illustrating the importance and influence of the appropriate winding design on the power output capability of the fixed-speed PM generator.

The most promising winding design for the minimum power loss at the rated operating point has been down selected for prototyping. Theoretical findings from the analysis have been compared against experimental data from hardware tests on a stator winding section showing close agreement.

I. INTRODUCTION

Manufacturability is an important aspect of electric machine design, particularly when a cost effective solution is envisaged and together with the machine's required performance and intended application is a major driver of initial design choices.

The majority of the power loss within an electrical machine is generated in the stator winding assembly. Hence, appropriate design of the stator winding assembly is particularly important if a high-performance, compact machine design is required. In this context, an open-slot stator with concentrated winding arrangements can provide a number of desirable features. These include high conductor/winding fill factor, compact end-windings, simplicity of manufacture, ease of assembly and superior thermal performance [1]-[4]. Since thermal performance is a critical factor limiting the power output of an electric machine, an improvement in heat transfer and reduction in generated power loss is very desirable.

A common practice when considering a low-loss winding design is to assure high winding slot fill factor [1]- [4]. This allows for the dc winding power loss to be reduced. However, the majority of electrical machines operate under time varying or alternating current (ac) excitation making the low-loss winding design more challenging. In particular, the undesirable ac winding effects present at ac operation need to be considered. These include the proximity and skin effects together with the eddy-currents resulting from interaction between the winding conductors and the time changing magnetic field from the rotation of the rotor [1]-[11], [17]-[22].

There are several techniques allowing for the reduction or mitigation of the ac winding loss component including the use of appropriate conductor profiles, conductor gauge/dimensions, conductor arrangement, e.g Litz wire and others [1]-[11], [17]-[22]. The wide body of work devoted to the ac winding power loss in electrical machines is largely focused on high-speed traction applications [7]-[9]. These

978-1-4799-5776-7/14/$31.00 ©2014 IEEE

variable-speed machines require a fine balance between the dc and ac winding loss components to provide a high-efficiency operating envelope.

In this paper a fixed-speed PM generator is considered with the research focus placed on the minimum power loss and low-cost winding design. The fixed speed operation allows for the winding design to be finely tuned satisfying the design requirements, some of which considered here include good manufacture repeatability, mechanical robustness and resilience to mechanical stress. The thermal dependence of the winding loss in the ac power loss analysis is investigated and accounted for, which is essential for accurate predictions of thermal behaviour and power output envelopes. The existing technique for adjusting the ac winding power loss with temperature [7] has been further developed in this paper to account for the winding loss component from rotation of the rotor. The proposed approach allows for computationally efficient and accurate correction of the ac winding loss with temperature and excitation current, which is essential in high-fidelity thermal analysis of electrical machines and devices.

The open-slot stator topology considered here accommodates a preformed winding, which is constructed using edge-wound coils formed by rectangular profiled conductors. Such a winding construction allows for an automated and cost effective manufacturing process to be employed. Several winding variants with different conductor dimensions have been analysed using the finite element method (FEM), accounting for the winding operating temperature. The FE power loss predictions have been supplemented with thermal analysis of the complete generator assembly using the equivalent circuit approach (ECA). Implications regarding the generator power output capability for the considered winding variants are discussed in detail. The most promising winding design for the minimum power loss at the rated operating point has been down selected for prototyping. Theoretical findings from the analysis have been compared against experimental data from hardware tests on stator winding section showing good agreement. Moreover, effects of the localised winding power loss on the thermal behaviour and power output capability of the generator have been presented. The results suggest that accounting for the localised winding loss has a significant impact on the performance predictions for the analysed PM generator design.

II. Generator Construction

The analysed PM generator is a compact, liquid-cooled, radial-flux, brushless topology with outer rotor and surface mounted PMs. The open-slot outer rotor generator topology has been chosen as this machine configuration significantly simplifies the manufacturing process and was preferred in the particular generator application. The generator's rated operating frequency is approximately 350Hz. The number of poles and slots is p = 10 and q = 12 respectively. Fig. 1 presents schematically the stator and rotor cross-section of the PM generator. The laminated stator and rotor core packs are made of SiFe (M250-35A), and the PM array utilises high temperature NdFeB (N42UH) with axially segmented pole pieces. Here, 10 PM segments per rotor pole piece was used. The double-layer concentrated winding arrangement adopted here utilises edge-wound coils with profiled rectangular copper (Cu) conductors. Fig. 2 shows the prototyped edge-wound coils together with a section of the stator laminated core pack. The complete generator assembly is fully enclosed with the stator inner bore set at a fixed temperature of 90^0C. This is realised by a liquid-cooled heat-sink via the mechanical shaft arrangement. Table I lists basic data of the PM generator. A section of the stator winding assembly (motorette) shown in Fig. 2 has been manufactured to provide

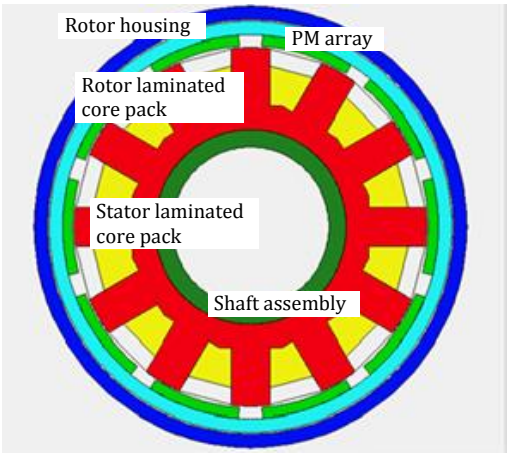

Fig. 1. Schematic cross-section of the PM generator

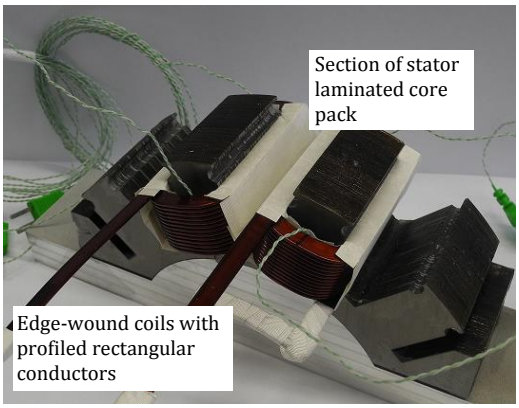

Fig. 2. Section of the stator laminated core pack together with the edge-wound coils – motorette assembly

TABLE I. BASIC MOTOR DATA

Outer diameter	250mm
Active length	51mm
Rated speed	4000rpm
Rated torque	72Nm
Rated current	$143A_{rms}$
Rated power	30kW

an initial evaluation for the winding power loss predictions and give some insight into the heat transfer effects, which are discussed later in the paper.

III. Mathematical Models

A. FEA-Electromagnetic Model

To achieve the minimum winding power loss requirement for the rated operation, a number of winding variants with different conductor sizes have been analysed by means of two- and three-dimensional (2D and 3D) FEM.

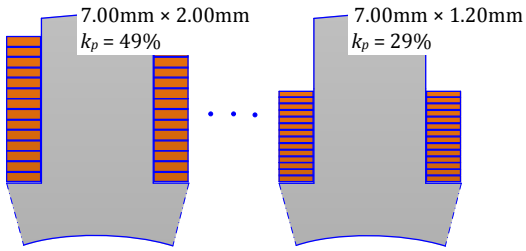

Fig. 3. Optional winding designs for various conductor dimensions, where k_p is the winding fill factor

Fig. 3 presents the two extremities of the winding variants considered, where the thickness of the winding conductors have been altered from 2.00mm to 1.20mm. In total, five conductor thicknesses were analysed with a conductor thickness step of 0.20mm between neighbouring variants. It is worth noting that the predicted winding fill factor (k_p) varies between 49% to 29% for the analysed conductor gauges.

The ac winding loss predictions have been made using time stepping FEA where the winding coils are driven with 3-phase sinusoidal and balanced current waveforms in the case of the complete generator assembly. The motorette model is driven with a 1-phase sinusoidal current waveform. The individual winding conductors are represented within the FE model as solid conductors linked with an external circuit defining electrical connections between the winding conductors, coils and phases where appropriate. The generated winding loss is determined from the Joule loss:

$$P = \iiint_V \boldsymbol{E}\cdot\boldsymbol{J}dV = \rho \iiint_V \boldsymbol{J}^2 dV = \rho l \iint_S J^2 dS \quad , \qquad (1)$$

where l is the equivalent active length, ρ is the electrical resistivity at the winding working temperature T and J is the current density.

To account for the change in copper resistivity with temperature, the following correction has been used in the FEA:

$$\rho|_T = \rho|_{T_0}\big(1+\alpha(T-T_0)\big), \quad , \qquad (2)$$

where $\rho|_{T_0}$ is the resistivity of copper at T_0 = 20°C, $1.7\times10^{-8}\Omega$m and α is temperature coefficient of resistance for Cu is $3.93 \times 10^{-3}\text{K}^{-1}$. The FEA assumes constant winding temperature T.

A commonly used figure of merit, when describing the ac winding loss is a ratio of the equivalent ac and dc resistance (R_{ac}/R_{dc}). This ratio defines the average winding power loss at ac operation and can be derived from hardware tests or FEAs assuming equivalent ac and dc excitation current (I) and fixed winding temperature, $(R_{ac}/R_{dc})|_{T,\,I} = (P_{ac}/P_{dc})|_{T,\,I}$ [7]. In this analysis R_{ac}/R_{dc} has been used to illustrate the ac winding effect as well as to define functional representation of the ac winding power loss with temperature, which is essential when thermal analysis is considered. It is important to note that the ac winding loss scales with temperature in a different manner than that at dc operation. In general, the winding power loss at ac operation can be represented as a superposition of three components:

$$P_{ac}(I,f,T) = P_{dc}(I,T) + P_{acE}(I,f,T) + P_{acR}(f,T) \quad , \qquad (3)$$

where P_{dc} is the dc winding loss component, P_{acE} is the ac winding loss component from the excitation current and P_{acR} is the ac winding loss from rotation of the rotor.

The existing technique of scaling the ac winding loss with temperature accounts for all these loss components [7]:

$$P_{ac}|_T = P_{dc}|_{T_0}\big(1+\alpha(T-T_0)\big) + P_{dc}|_{T_0}\frac{\left(\frac{R_{ac}}{R_{dc}}\right)\Big|_{T_0} - 1}{\big(1+\alpha(T-T_0)\big)^{\beta}} \quad , \qquad (4)$$

where

$$P_{dc}|_{T_0} = I^2 R_{dc}|_{T_0} \quad . \qquad (5)$$

The parameter β can be found by curve fitting (4) into the ac winding loss data for temperature T. It has been assumed here that T is the highest operating temperature considered for a device.

It is important to note that the second term in (4) accounts for all winding ac loss components listed in (3) by means of R_{ac}/R_{dc} ratio. However, as the P_{acR} depends on the rotational speed/frequency and winding temperature only, an adjustment of P_{ac} with the excitation current requires additional FEAs. To eliminate the necessity of FEAs for optional excitation currents a generalised form of (4) has been

introduced:

$$P_{ac}|_T = P_{dc}|_{T_0}\left(1+\alpha(T-T_0)\right) + P_{dc}|_{T_0}\frac{\left(\frac{R_{ac}}{R_{dc}}\right)_E\Big|_{T_0}-1}{\left(1+\alpha(T-T_0)\right)^{\beta}} + P_{acR}|_{T_0}\frac{1}{\left(1+\alpha(T-T_0)\right)^{\gamma}} \quad , \qquad (6)$$

where

$$\left(\frac{R_{ac}}{R_{dc}}\right)_E\Big|_{T,I} = \left(\frac{P_{ac}-P_{acR}}{P_{dc}}\right)\Big|_{T,I} \quad , \qquad (7)$$

and P_{acR} is the winding loss at open-circuit operation and the parameter γ can be found by curve fitting the last component of (6) into the open-circuit ac winding loss data for temperature T. Similarly as in (3) T is the highest operating temperature considered for a device.

The proposed approach (6) allows for simple adjustment of the ac winding loss with both the temperature and excitation current. It is important to note that the technique is accurate if the magnetic saturation effects within the machine's magnetic circuit are negligible, i.e. R_{ac}/R_{dc} is independent on the excitation current, which is the case for the analysed machine. Also, if P_{acR} is negligibly small, (6) is equivalent to (4), and no open-circuit winding loss FEA is required.

When deriving the ac winding power loss using either experimental or theoretical approach, an averaged/lumped loss over the entire winding assembly or active length is usually considered. However, to account for the active length and end winding loss contributions in thermal analysis, a loss separation for these two regions is required. This is particularly important for machine designs with relatively short active length, as is the case here, where the end-winding contribution to the overall winding loss is significant.

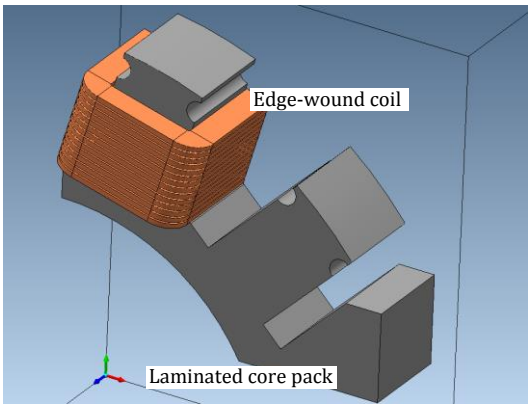

Fig. 4. 3D FEM model representation of the motorette assembly

A commonly used approach of separating the active length and end winding loss is based on average winding/conductor length, which is applicable for dc winding loss only. When considering winding loss at ac operation, the mechanisms responsible for the losses seen in these two discrete regions are dissimilar [5]. Consequently, the winding regions need to be analysed individually [5], [7].

In this analysis, 3D FEA has been employed to give some insight into the ac end-winding loss contribution. Fig. 4 shows a 3D model representation of the motorette assembly. Note that due to geometrical symmetry only one quarter of the motorette has been analysed. Results from 3D FEA of the motorette has been used to correct for the end-winding effects for the complete generator assembly analysed using a 2D approach.

Further to the winding loss separation for the active length and end-winding regions a more detailed approach has been introduced. Here, the loss generated in the individual winding layers/conductors is considered to give some insight into the winding localised power loss phenomena. These clearly have some detrimental effects on the generator thermal behaviour and consequently power output capability, which are discussed later in the paper. It is worth noting that the localised winding loss is expected to be significant for the analysed generator topology due to specifics of the open-slot stator and edge-wound winding design.

Both the winding power loss representations considered here can be expressed in the following form

$$P_{ac} = P_{ac\,al} + P_{ac\,ew} \Rightarrow \sum_{i=1}^{nl}(P_{ac})_i = \sum_{i=1}^{nl}(P_{ac\,al})_i + \sum_{i=1}^{nl}(P_{ac\,ew})_i \quad , \qquad (8)$$

where $P_{ac\,al}$ and $P_{ac\,ew}$ refers to the active length and end-winding region respectively, index i corresponds to the i-th winding layer and nl is the number of the winding layers within the stator slot, here nl = 14. Each of the winding regions has its own loss function (6) with appropriate $[(R_{ac}/R_{dc})_E]_i$, $(\beta)_i$ and $(\gamma)_i$ data derived from the FEAs. It is important to note that the ac end-winding loss from rotation of the rotor has been assumed negligible and is not considered in the analysis.

The winding power loss predictions have been supplemented with the iron and PM power loss data from the FEAs used later in the thermal ECA of the complete generator assembly. The mechanical power loss component has been assumed based on data provided by the bearing manufacturer. Here, for reasons of conciseness the supplementary loss components are not discussed. However, the authors' previous works provides an insight into the

techniques for deriving these loss components [1]-[3], [5] also used in this research.

B. ECA – Thermal Model

A complete thermal model of the PM generator has been built using the thermal ECA [13]. The model caters for the conduction, convection and radiation heat transfers including the air-flow transition effects. Fig. 5a presents the thermal network used, where colors indicate parts of the motor assembly, see also Fig. 1. To accommodate for the detailed winding power loss data discussed earlier, a winding model representation utilising cuboidal elements has been employed here. A cuboidal element allows for an accurate 3D EC model representation accounting for the internal heat generation and material thermal anisotropy [15]. Each of the individual winding layers/conductors within the EC model is represented by the cuboidal element together with corresponding loss function (6). For the averaged/lumped winding loss representation, the winding loss for the individual layers/conductors is identical, whereas the more detailed loss representation accounts for inhomogeneous loss distribution between the winding layers.

a)

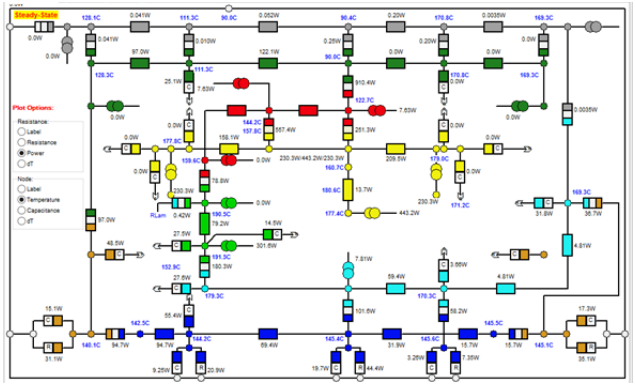

b)

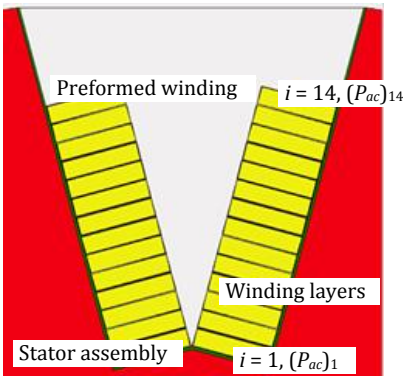

Fig. 5. Thermal EC model representation of the PM generator assembly a) lumped-parameter thermal network, b) stator slot with individual winding layers

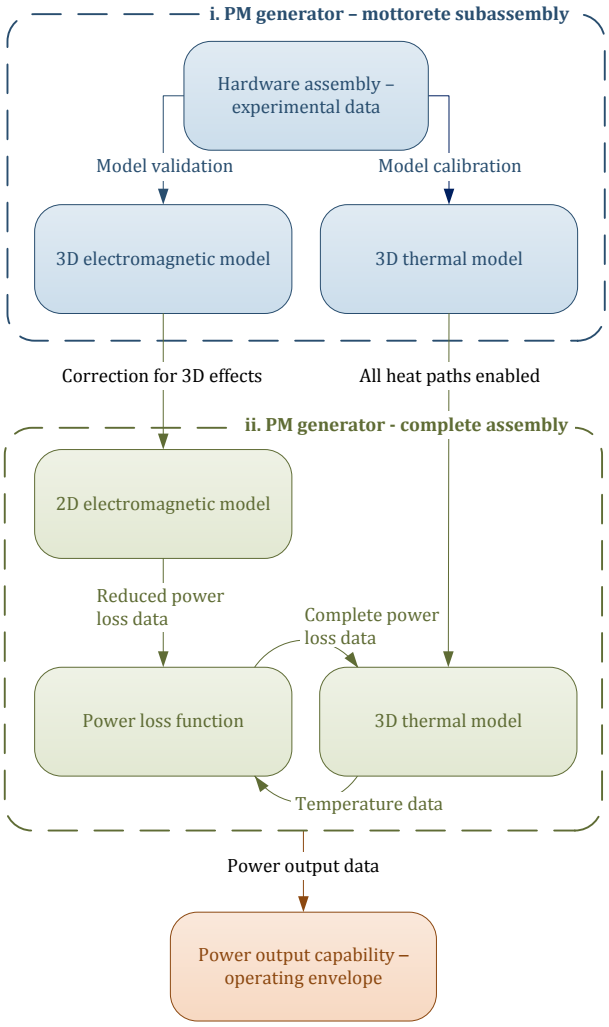

Fig. 6. Flow chart for the coupled electromagnetic and thermal analysis

To provide a degree of calibration for the thermal model, a dc test on the motorette assembly has been carried out. The aim of the test was to determine the quality of the conductive heat transfer path from the winding throughout the stator core pack into the heat sunk shaft assembly. It is important to note that for the purpose of this initial calibration, other heat transfer mechanisms such as, convection and radiation, are assumed to be negligible. This has been realised by thermally insulating the motorette surfaces, which are not in contact with the cold plate assembly. Details regarding the experimental setup used in dc test are given in the next section.

An initial sensitivity analysis has been performed using the thermal EC model to identify the main heat transfer paths and mechanisms together with construction/assembly nuances, which have a significant impact on the generator thermal behaviour. The analysis confirmed that the main heat transfer path is provided by conduction from the impregnated stator/winding assembly to the heat sunk shaft. As this is the intended mechanism for evacuating heat from the generator body, correct calibration of any interface thermal resistances

from the stator/winding to the motor shaft were found to be crucial to the accuracy of the thermal model. The calibrated model is the basis for the analysis of the generator power output capability for the different winding variants.

C. Coupled Electromagnetic and Thermal Analysis

The complete coupled electromagnetic and thermal analysis of the PM generator employs the modelling techniques and approaches discussed in the earlier sub-sections of the paper. A flowchart outlining sequence of the theoretical and experimental activities used in the process of setting up the coupled analysis is shown in Fig. 6. There are two main stages to the overall process. In stage (i.) the motorette hardware assembly is used to calibrate thermal model of the machine and validate power loss derivation methods. The initial power loss analysis allows for the 3D effects to be quantified and corrected for in the later 2D analysis of the complete PM generator assembly. It is important to note that the thermal model used in stage (i.) is based on complete thermal network of the PM generator with appropriate heat paths being disabled, allowing for the motorette assembly to be emulated/analysed. In stage (ii.) complete assembly of the generator is considered. The 2D electromagnetic model with correction for the 3D effects is used to generate the power loss function allowing for computationally efficient thermal analysis without need for further FEAs. The calibrated thermal model with complete thermal network, all heat paths are enabled in this case, is coupled with the power loss function allowing for the iterative power loss and temperature updates. Deterioration of the PM generator performance caused by elevated temperature of the PM material is also accounted for in the coupled analysis.

IV. Experimentation

A. DC Test – Heat TransferAnalysis

To provide an initial insight into the heat transfer from the generator stator/winding assembly to the heat sunk shaft, a dc test was carried out on the motorette setup. The motorette body was mounted on a liquid-cooled aluminum interfacing plate with appropriate retention system to emulate the shaft assembly. Fig. 2 presents the motorette body together with the interfacing plate prior to the final assembly. It is important to note that only the motorette's stator inner bore surface is in contact with the interfacing plate. The remaining parallel surfaces between the motorette's stator and interfacing plate are thermally insulated during the tests. The motorette setup is then placed in a thermally insulated chamber and instrumented with type-K thermocouples. Excitation for the motorette winding is provided by a dc power supply, and the fixed temperature of the cold plate is controlled by a cooling unit. The temperature within the motorette assembly was monitored at a number of points including the winding, laminated core pack, aluminum interfacing plate and cold plate. The measurements were taken for several excitation currents, and the averaged test data was used to calibrate the thermal model. The complete experimental setup used for the dc test is shown in Fig. 7.

B. AC Test – Power Loss Measurements

In order to derive the ac winding loss an experimental rig shown in Fig. 8 has been set up. The tests were undertaken to assess the copper loss generated within the motorette assembly under 1-phase ac operation for various excitation frequencies and winding temperatures. The mottorette was excited by a custom built 1-phase IGBT variable frequency voltage source inverter (VSI), the output of which was low-pass filtered to provide sinusoidal voltage and load current. The mean winding temperature was manually controlled to within ±2°C by applying an additional excitation current in-between test points. The temperature within the windings was monitored at a number of points to provide an averaged temperature reading. These temperature measurements were taken using type-K thermocouples. The temperature and copper loss was monitored simultaneously allowing for accurate readings accounting for the temperature change.
The power loss was measured using a high bandwidth power analyser together with precision current transducers.

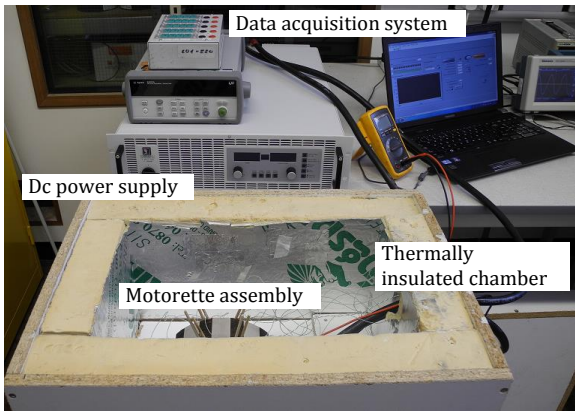

Fig. 7. Experimental test setup for the dc tests

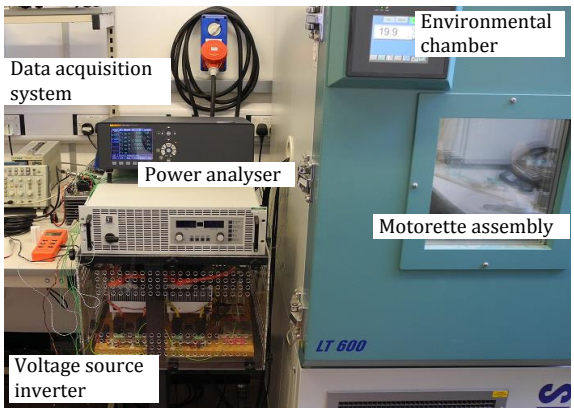

Fig. 8. Experimental test setup for the ac tests

The complete list of instrumentation used in the testing

includes: a high bandwidth power analyser (Norma 5000), high accuracy (+/-0.003%) current transducers (LEM IT 400S) and a thermal data acquisition system (Agilent 34980A).

V. Results and Discussion

Initial FEAs of the PM generator have shown that the eddy-current losses induced in the stator winding as a result of the time-changing field from rotation of the PM rotor assembly is the dominant component of the winding loss at ac operation. This is caused by the open-slot stator-winding construction, which encourages elevated winding loss from the PM rotor. Fig. 9 presents FE predictions of the winding power loss components at maximum torque per Ampere operation of the generator to illustrate this effect. The loss analysis has been carried out for several winding variants utilising different conductor dimensions. Here, only the thickness of the copper winding conductors was changed between analyses. The reduced conductor thickness results in the winding conductors being placed lower in the stator slots as is shown in Fig. 3.This leads to reduced winding loss from the PM rotor as the winding conductors are less exposed to change of the magnetic field generated by the rotating rotor assembly. Also, to provide a more generic insight into the winding ac effects a number of rotational speeds has been considered. The FE results suggest that for $n > 0$ the winding construction with reduced conductor thickness, reduced winding fill factor k_p provides lower winding power loss than the counterparts with relatively high winding fill factor analysed in this research. This might be counterintuitive if the more common dc winding resistance or winding fill factor design criteria are taken into account only. Also, when inspecting the results it is clear that the skin and proximity effects are insignificant in the analysed PM generator. The winding loss predictions from the excitation current P_{acE}, show moderate winding loss increase with the operating speed/frequency. It is important to note that in some machine designs the use of magnetic slot closure emulating a semi-closed slot design might be feasible, which allows for the rotational winding loss component, P_{acR}, to be significantly reduced. This results from the shielding effect of the magnetic slot closure for the winding conductors. However, the proximity of the magnetic wedge material to the winding conductors might encourage elevated ac winding loss from excitation, P_{acE}, due to increased flux leakage at the slot opening. Also, power loss in the magnetic wedges exposed to severe changes of the magnetic flux in the air-gap region requires careful consideration. Though, the use of magnetic slot closure/wedge solution has not been considered in this analysis.

As the winding loss at ac operation changes with temperature in a different manner than that at dc excitation (6) it is crucial to account for the temperature effects in the winding loss analysis.

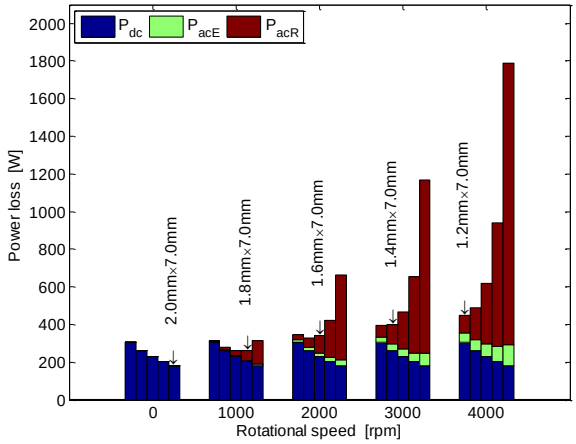

Fig. 9. Winding power loss components versus rotational speed at rated current $I = 143A_{rms}$ and winding temperature $T = 20°C$

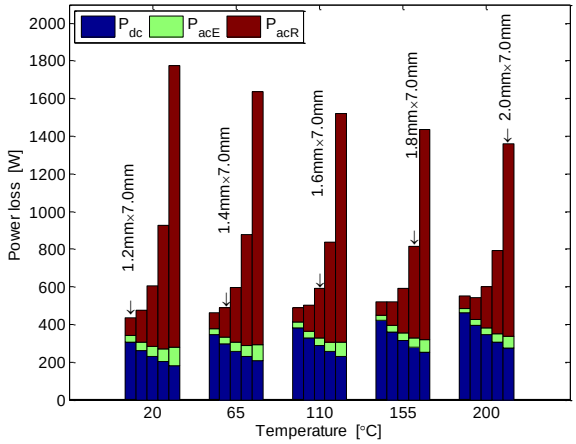

Fig. 10. Winding power loss versus winding temperature at rated operating point, $I = 143A_{rms}$, $n = 4000$rpm

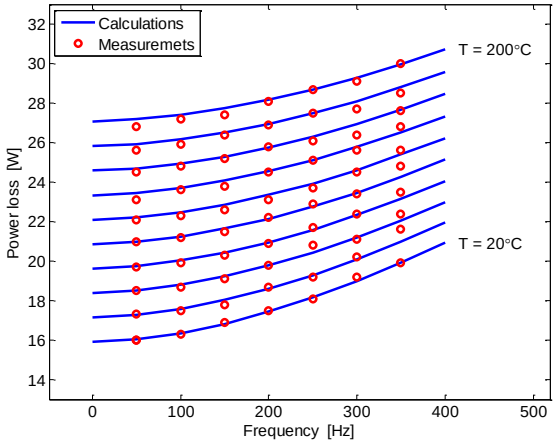

Fig. 11. Measured and calculated total power loss versus excitation frequency for the motorette assembly at excitation current $I = 40A_{rms}$ – winding variant with conductor dimensions 1.5mm × 7.0mm

In this investigation winding variants within the range of conductor dimensions 1.6mm × 7.0mm and 1.2mm × 7.0mm provide the lowest winding power loss for the winding operating temperature limit set at 180°C, Fig. 10. It is important to note that the results shown in Fig. 10 refer to the generator rated operating point, $I = 143A_{rms}$ and $n = 4000$rpm. Based on this initial analysis, the winding variant with conductor dimensions 1.5mm × 7.0mm has been down-selected for prototyping.

To gain a more in depth understanding of the ac winding power loss for the active length and end-winding regions, the 3D FEAs and tests on the motorette assembly have been carried out. Initially, the accuracy of the employed 3D FEA has been evaluated. Fig. 11 presents total power loss generated within the motorette assembly for various excitation frequencies and winding temperatures. The theoretical loss predictions show good agreement with the test data. It is important to note that the total power loss referred to here, includes both the iron and winding loss components. This provides a validation for the employed theoretical techniques for the power loss predictions. The loss variation with temperature shown in Fig. 11 is attributed here to a change of the winding electrical resistivity. However, in general, the iron loss is also temperature dependent [16], but in this analysis this effect has not been accounted for. The FE models used in this analysis cater for the winding loss temperature dependence only.

Fig. 12 presents FE predictions of R_{ac}/R_{dc} ratio for the moterette assembly. Both the active length and end-winding region contributions are shown. The results suggest insignificant ac effects for the end-winding region, particularly at elevated winding temperatures. It is important to note that the moterette FEAs do not account for the interactions between neighbouring phases or the rotating PM rotor contribution to the overall winding loss.

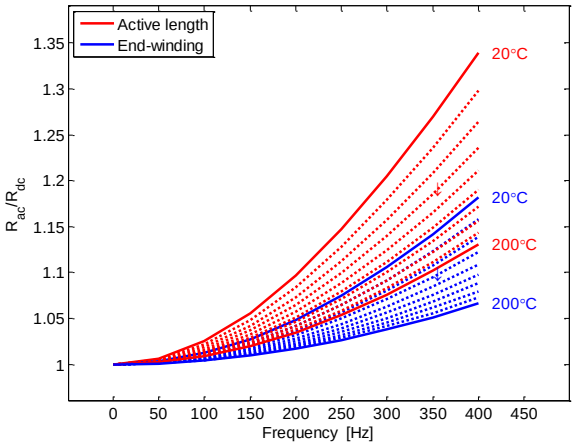

Fig. 12. R_{ac}/R_{dc} ratio versus excitation frequency for the motorette assembly at excitation current $I = 40A_{rms}$ - winding variant with conductor dimensions 1.5mm × 7.0mm

a)

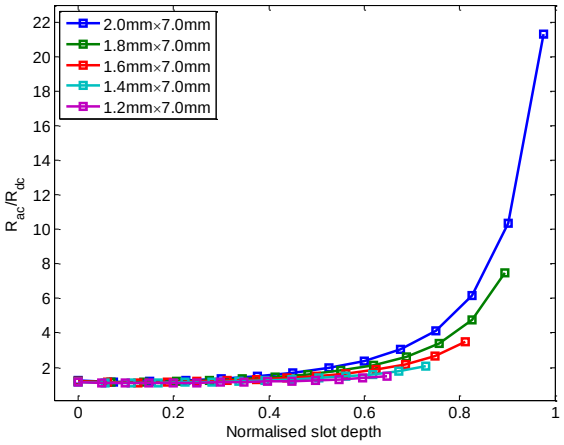

b)

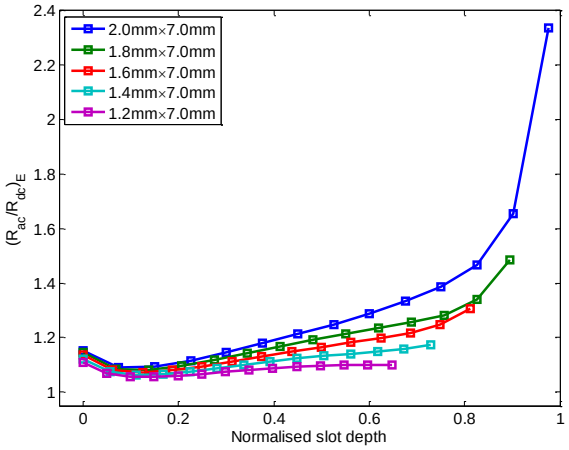

Fig. 13. R_{ac}/R_{dc} ratio for winding active length versus normalised slot depth at rated operating point, $I = 143A_{rms}$, $n = 4000$rpm and winding temperature $T = 200$°C a) R_{ac}/R_{dc}, b) $(R_{ac}/R_{dc})_E$

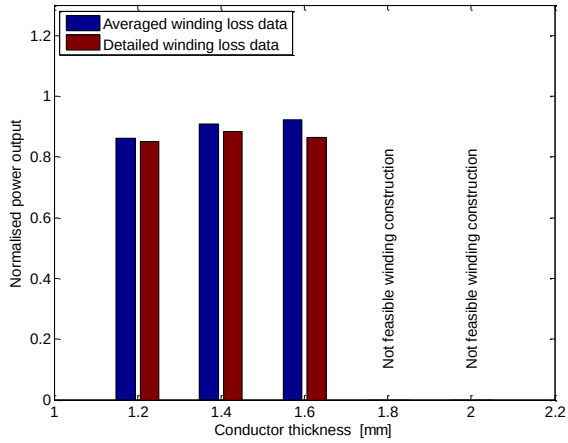

Fig. 14. Normalised power output versus conductor thickness for 180°C winding temperature limit

These are particularly important for accurate winding loss predictions for the winding active length region, see Figs. 9 and 10. However, it is expected that for the analysed generator, these effects have minor impact on the end-winding region. Thus the end-winding loss predictions from the motorette analysis for the optional conductor dimensions have been used to adjust the 2D winding loss results of the complete generator.

The winding loss or R_{ac}/R_{dc} ratio data is usually averaged over the entire winding region or volume. Such an approach does not provide any information regarding inhomogeneous distribution of the loss within the winding assembly. This might lead to significant discrepancies in predictions of the machine thermal behaviour and/or power output capability. In the analysed generator, the localised winding loss issue is particularly prominent for the winding variants with relatively high winding fill factor. Fig. 13 presents R_{ac}/R_{dc} ratio for the individual winding layers of the analysed generator versus normalised slot depth, where 0 corresponds to bottom of the stator slot (stator back iron), and 1 is the top layer within the stator slot (stator slot opening), see Fig. 5. The square markers shown in Fig. 13 represent the individual winding layers location within the stator slot. Both the R_{ac}/R_{dc} and $(R_{ac}/R_{dc})_E$ are presented, where the first one represent the overall winding loss at ac operation, Fig. 13a, and the second one represent the winding loss without the rotor reaction effect, Fig. 13b. It is evident that the top layers of the winding generate significantly higher power loss than these placed lower in the stator slot, see Fig. 13a. As it has been identified earlier this is attributed to the rotating PM rotor effect. Also, the results for the individual winding layers confirm that winding construction, where the top winding layer is placed below 0.8 of the normalised stator depth provides low winding loss at ac operation. Fig. 13b shows $(R_{ac}/R_{dc})_E$ ratio, which accounts for the ac effects from the current excitation only indicating moderate increase of the dc winding resistance at ac operation. Note that due to elevated flux linkage at the slot opening, the conductors placed higher in the slot exhibit greater ac loss even if the excitation effects are accounted for only.

The power output capability of the generator has been evaluated using the thermal EC model discussed earlier, assuming the rated operating speed and adjusting the excitation current to respect the 180°C winding temperature limit, Fig. 14. The results suggest that the winding variant with conductor dimensions 1.4mm × 7.0mm provides the minimum winding power loss and 88% of the target rated power output capability, table I. The performance is expected to be improved if a vacuum impregnation technique is employed in place of the dip varnish method used in this analysis. Also, the results indicate that the winding variants with relatively high winding fill factor considered here, 2.0mm × 7.0mm and 1.8mm × 7.0mm are not feasible due to prohibitive winding loss generated. Moreover, the results show the impact of the localised winding power loss on the power output predictions for the winding variants considered. The averaged winding loss approach overpredicts the generator power output capability. This is particularly prominent for the winding variants where the inhomogeneous winding power loss distribution is significant, see Fig. 14. Here, the power output capability is overpredicted by 7% for the worst case. The power output predictions for the winding variants with evenly distributed generated loss between winding layers for both the averaged and detailed winding loss representation are closely matched.

VI. Conclusions

This paper outlines the design of a winding for minimum power loss at ac operation in application to a fixed-speed PM generator. The fixed speed operation allows for the winding design to be finely tuned satisfying numerous design requirements, some of which include low-cost manufacture, good manufacture repeatability, mechanical robustness and resilience to mechanical stress. An edge-wound pre-formed concentrated winding design utilising profiled rectangular Cu conductors has been considered here. Such a winding construction allows for an automated coil forming process to be employed lowering the manufacture and assembly cost. Also, the material cost for the profiled rectangular winding wire is substantially lower than the alternative low-loss conductor arrangements, e.g. compacted type-8 Litz wire with equivalent insulation class, considered in the design trade study. The wire cost for the same winding fill factor is £8.0 per meter for the type-8 Litz as compared with £0.7 for the profiled rectangular solution. However, it is important to note that the high purchase volume pricing is not considered here.

The proposed winding design-analysis accounts for the detailed winding power loss distribution with distinction for the individual winding conductors/layers for both the active length and end-winding regions. The temperature dependence of the winding loss at ac operation has also been incorporated in the investigation. The calculated results have shown that accounting for the thermal and localised winding loss effects is crucial in making an informed decision regarding the low-loss winding construction, and more commonly used approach where winding fill factor or averaged winding loss is considered only might not yield required accuracy.

From the analysis of numerous winding variants, the most promising winding design has been down selected and prototyped. It has been confirmed that the edge-wound winding construction provides a low-loss solution when considering ac effects from excitation. However, in context of the open-slot stator topology, careful considerations must be taken to identify and quantify the ac loss from rotation of the rotor assembly. This effect is frequently overlooked in analysis of more conventional machine topologies, but in some cases can be prohibitively high as it has been shown in the paper. The theoretical predictions from the design/modelling techniques used in the research have been supplemented with hardware tests on the motorette assembly. The motorette assembly allows for cost and time effective evaluation of hardware elements that are of particular interest; here the stator/winding assembly has been investigated. Data from the moterette tests has been used to validate the methodology employed in the design process and to give an insight into nuances of the heat transfer and loss effects, which

are notoriously difficult to derive using purely theoretical methods. It has been shown that the theoretical findings are in close agreement with the test results.

Moreover, the existing technique for adjusting the ac winding power loss with temperature has been further developed in the paper to account for the winding loss component from rotation of the rotor. The proposed approach allows for computationally efficient and accurate adjustment of the ac winding loss with temperature and excitation current, which is essential in thermal analysis of electrical machines and devices.

ACKNOWLEDGMENT

The authors wish to thank Infolytica Europe for providing the FEM software used in this research. The authors also wish to acknowledge that the work presented in this paper was supported jointly by the AgustaWestland and EC through the FP7 JTI Clean Skies programme (HERRB Project, Grant code: JTI-CS-2011-01-GRC-03-007).

REFERENCES

[1] R. Wrobel, P. H. Mellor, "Design Considerations of a Direct Drive Brushless Machine with Concentrated Windings," *IEEE Transactions on Energy Conversion*, vol. 23, no. 1, pp. 1 – 8, March 2008.

[2] R. Wrobel, P. H. Mellor, D. Holliday, "Thermal Modelling of a Segmented Stator Winding Design," *IEEE Transactions on Industry Applications*, vol. 47, no. 5, pp. 2023 – 2030, September – October 2011.

[3] R. Wrobel, P. H. Mellor, N. McNeill, D. A. Staton, "Thermal Performance of an Open-Slot Modular-Wound Machine with External Rotor," *IEEE Transactions on Energy Conversion*, vo. 25, no. 2, pp. 403 – 411, June 2010.

[4] P. Arumugam, T. Hamiti, C. Gerada, "Modeling of Different Winding Configurations for Fault-Tolerant Permanent Magnet Machines to Restrain Interturn Short-Circuit Current," *IEEE Transactions on Energy Conversion*, vol. 27, no. 2, pp. 351 – 361, June 2012.

[5] R. Wrobel, A. Mlot, P. H. Mellor, "Contribution of End-Winding Proximity Losses to Temperature Variation in Electromagnetic Devices," *IEEE Transactions on Industrial Electronics*, vol. 59, pp. 848-857, February 2012.

[6] S. Iwasaki, R. P. Deodhar, L. Yong, A. Pride, Z. Q. Zhu, "Influence of PWM on Proximity Loss in Permanent-Magnet Brushless AC Machines," *IEEE Transactions on Industry Applications*, vol. 45, pp. 1359-1367, July/August 2009.

[7] R. Wrobel, A. Griffo, P. H. Mellor, "Derivation and Scaling of AC Copper Loss in Thermal Modeling of Electrical Machines," *IEEE Transactions on Industrial Electronics*, vol. 61, pp. 4412 – 4420, August 2014.

[8] P. B. Reddy, T. M. Jahns, "Analysis of Bundle Losses in High Speed Machines," *International Conference on Power Electronics*, 2010, *IPEC'10*, pp. 2181-2188.

[9] P. H. Mellor, R. Wrobel, McNeill, "Investigation of Proximity Losses in a High Speed Brushless Permanent Motor," *41st IAS Annual Meeting, IEEE Industry Applications Conference, 2006*, vol. 3, pp. 1514 – 1518, September 2006.

[10] L. J. Wu, Z. Q. Zhu, D. Staton, M. Popescu, D. Hawkins, "Analytical Model of Eddy Current Loss in Windings of Permanent-Magnet Machines Accounting for Load," *IEEE Transactions on Magnetics*, vol. 48, no. 7, pp. 2138 – 2151, July 2012.

[11] Y. Amara, P. Reghem, G. Barakat, "Analytical Predictions of Eddy-Current Loss in Armature Winding of Permanent Magnet Brushless AC Machines," *IEEE Transactions on Magnetics*, vol. 46, no. 8, pp. 3481 – 3484, August 2010.

[12] H. Hamalainen, J. Pyrhonen, J. Nerg, "AC Resistance Factor in One-Layer Form-Wound Winding Used in Rotating Electrical Machines," *IEEE Transactions on Magnetics*, vol. 49, no. 6, pp. 2967 – 2973, June 2013.

[13] Motor-CAD V6 Maual, Motor Design Ltd, 2011.

[14] R. Wrobel, J. Goss, A. Mlot, P. H. Mellor, "Design Considerations of a Brushless Open-Slot Radial-Flux PM Hub Motor," *IEEE Transactions on Industry Applications*, vol. 50, pp. 1757-1757, May/June 2014.

[15] R. Wrobel, P. H. Mellor, "A General Cuboidal Element for Three-Dimensional Thermal Modelling," *IEEE Transactions on Magnetics*, vol. 46, pp. 3197-3200, August 2010.

[16] A. Mouillet, J. L. Ille, M. Akroune, M. A. Dami, "Magnetic and Loss Characteristics of Nonoriented Silicon-Iron Under Unconventional Conditions," *IEE Proceedings of Science, Measurement and Technology*, vol. 141, pp. 75-78, January 1994.

[17] L. J. Wu, Z. Q. Zhu, "Simplified Analytical Model and Investigation of Open-Circuit AC Winding Loss of Permanent-Magnet Machines," *IEEE Transactions on Industrial Electronics*, vol. 61, no. 9, pp. 4990 – 4999, September 2014.

[18] Z. Wanjun, T. M. Jahns, "Analytical 2-D Slot Model for Predicting AC Losses in Bar-Wound Machine Windings due to Armature Reaction," *IEEE Trasnsportation Electrification Conference and Expo*, 2014, *ITEC'14*, pp. 1 – 6.

[19] M. Vetuschi, F. Cupertino, "Minimization of Proximity Losses in Electrical Machines with Tooth-Wound Coils," *IEEE Transactions on Industry Applications*, pp. 1 – 9, March 2015 (*early acess paper*).

[20] D. A. Gonzalez, D. M. Saban, "Study of the Copper Losses in a High-Speed Permanent-Magnet Machine with Form-Wound Windings," *IEEE Transactions on Industrial Electronics*, vol. 61, no. 6. Pp. 3038 – 3045, June 2014.

[21] M. van der Geest, H. Polinder, J. A. Ferreira, D. Zeilstra, "Current Sharing Analysis of Parallel Strands in Low-Voltage High-Speed Machines," IEEE Transactions on Industrial Electronics, vol. 61, no. 6, pp. 3064 – 3070, June 2014.

[22] D. C. Hanselman, W. H. Peake, "Eddy-Currents Effects in Slot-Bound Conductors," *Electric Power Applications - IEEE Proceedings*, vol. 142, no. 2, pp. 131-136, 1995.